Journal of Microscopy

Journal of Microscopy, Vol. 00, Issue 00 2019, pp. 1–5
Received 29 June 2019; accepted 7 November 2019

doi: 10.1111/jmi.12845

In situ heating TEM observations of evolving nanoscale Al–Mg–Si–Cu precipitates

JONAS KRISTOFFER SUNDE*, SIGURD WENNER† & RANDI HOLMESTAD*
*Department of Physics, Norwegian University of Science and Technology (NTNU), Trondheim, Norway
†Materials and Nanotechnology, SINTEF Industry, Trondheim, Norway

Key words. Aluminium alloys, *in situ* transmission electron microscopy, phase mapping, precipitation, scanning precession electron diffraction.

Summary

This research concerns the precipitation and subsequent dissolution of precipitate phases in an Al–0.86Mg–0.62Si–0.1Cu (at.%) alloy subjected to varying thermal exposure during an *in situ* heating transmission electron microscope (TEM) experiment. The distribution and crystal structure of precipitates were determined by a scanning diffraction approach at multiple stages, pinpointing the precipitates that underwent phase transformations during heating. Obtained results were compared with TEM studies of the material heated *ex situ*. This revealed differences in the transformation kinetics of precipitates in an electron transparent lamella (thickness $\gtrapprox 90$ nm) to that of macroscopic bulk specimens.

Introduction

Age-hardenable Al alloys are an important group of structural materials that are strengthened by nanosized, metastable precipitates formed during thermal ageing. The precipitates are conventionally studied using the TEM, with electron transparent specimens prepared from materials heat treated to different stages. Due to improvements in specimen preparation techniques and the advent of TEM heating holders with high mechanical and thermal stability, it has now become possible to study the evolution of precipitates *in situ* (Malladi *et al.*, 2014; Liu *et al.*, 2017; Park *et al.*, 2019).

Al–Mg–Si(–Cu) alloys are important in automotive and construction applications, and form characteristic needle- or lath-shaped precipitates with long axes parallel to $<100>_{\mathrm{Al}}$ upon ageing (Edwards *et al.*, 1998; Marioara *et al.*, 2007). Previous *in situ* heating studies of precipitates in this alloy system have measured the overall changes to the distribution of precipitate parameters (lengths, densities, etc.) (Tsao *et al.*, 2006; Chang *et al.*, 2015; Flament *et al.*, 2017). We have here conducted an *in situ* heating TEM study, using bright-field imaging and scanning precession electron diffraction (SPED) combined with data post-processing to study the distribution and identities of transforming precipitates. A single region of interest was systematically studied, enabling tracking of the evolution of individual precipitate phases. The results were compared to conventional TEM studies of the material heat treated *ex situ* (Sunde *et al.*, 2019).

Correspondence to: Jonas Kristoffer Sunde, Department of Physics, NTNU, N-7491 Trondheim, Norway. Tel: +47 90918060; e-mail: jonas.k.sunde@ntnu.no

Material and methods

An extruded Al–0.86Mg–0.62Si–0.1Cu (at.%) alloy was subjected to solution heat treatment (SHT) at 540°C for 12 min, and subsequently water-quenched to room temperature (RT). The specimens heat treated *ex situ* were kept 10 min at RT before artificial ageing at 180°C. A peak-hardened material was obtained after approximately 3 h ageing. TEM specimens were made by standard electro-polishing using a Struers Tenupol-5 applying a 1:2 nitric acid:methanol mixture ($T \approx -25$°C).

Electron backscatter diffraction was conducted in a Hitachi SU6600 FE scanning electron microscope (SEM) on an electropolished TEM specimen which enabled mapping and identification of grains close to $\langle 001 \rangle_{\mathrm{Al}}$ orientation. The specimen had been heat treated 20 min at 180°C *ex situ* to initiate the precipitation in bulk conditions. Subsequently, a focused ion beam (FIB) lamella of a $\langle 001 \rangle_{\mathrm{Al}}$-oriented grain was prepared and mounted on a DENSsolutions nanochip using a FEI Helios G4 FIB. The chip was placed in a DENSsolutions D6 wildfire TEM holder which kept the specimen at 180–240°C in-between SPED scans. A JEOL 2100F microscope (200 kV) was used to run the *in situ* heating and SPED experiments. SPED was conducted using a NanoMEGAS ASTAR system. The nanobeam diffraction probe semi-convergence angle was 1.0 mrad and the precession angle employed was 1.0°. The scan step size was selected as 1.52 nm and pixel exposure time was 40 ms. SPED scans were recorded with the temperature held at RT ($T = 23$°C) and typically comprised 400 × 400 pixels, thus covering an area of ~600 × 600 nm^2 and taking

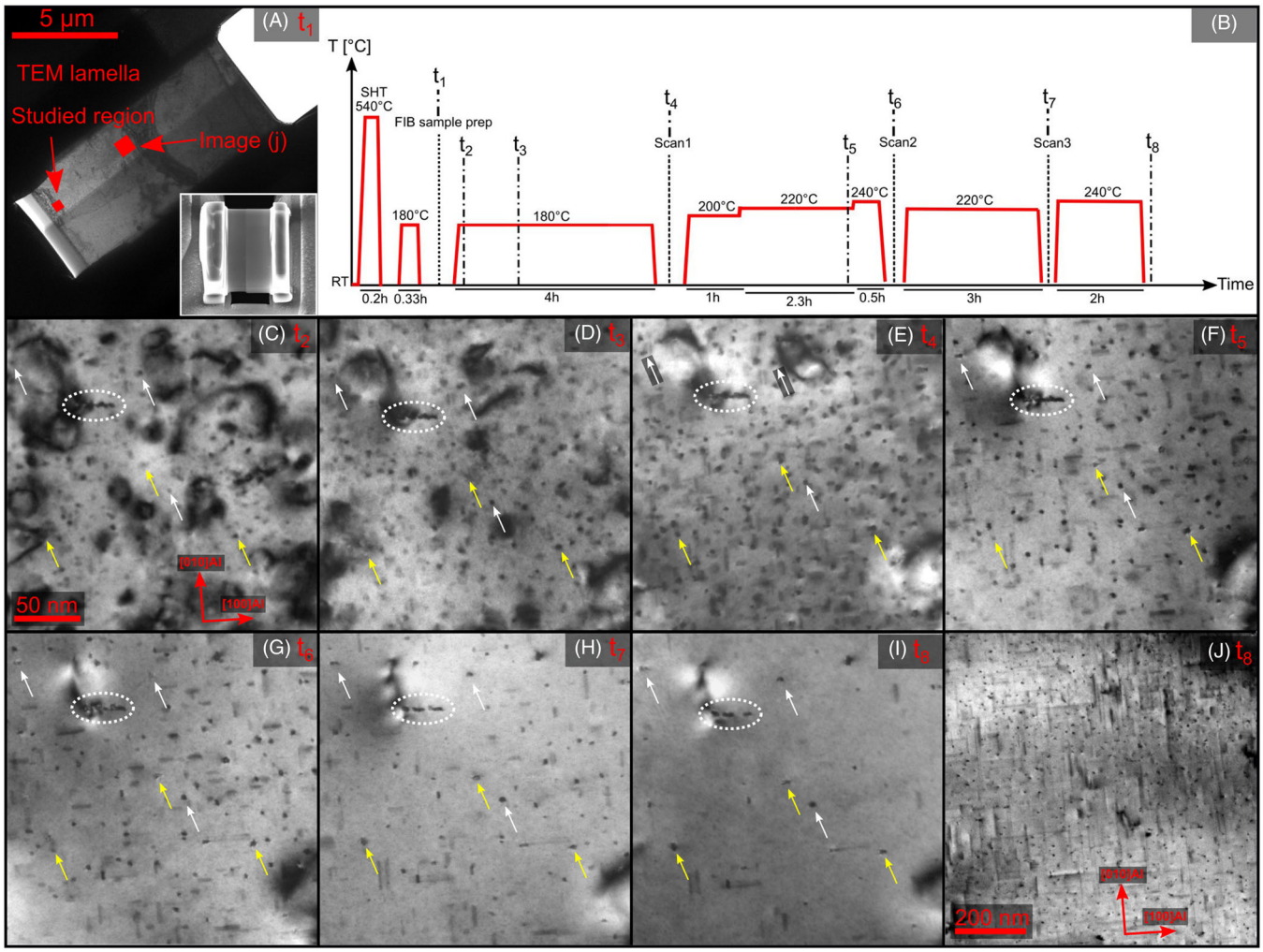

Fig. 1. (A) TEM image of the FIB prepared lamella. Insert shows a SEM image of the ion-milled lamella mounted across the heating holder SiN window using a C-weld. (B) A schematic of the heat treatment procedure. (C–I) Bright-field images acquired at indicated times (t_x) in the region highlighted in image (A) (~90nm thickness). White and yellow arrows indicate *L* and (β''/)β'/*Q*′ phases, respectively, that remain in the studied region after all stages of heating. The white dashed oval highlights coarsened precipitates that have formed on an underlying dislocation, and acts as a point of reference between images. (J) Bright-field image acquired in the indicated region of image (A) (~130 nm thickness).

approximately 1.5 h to acquire. Specimen thickness was measured by electron energy loss spectroscopy. The obtained 4D SPED datasets, comprising a 2D PED pattern at each position of a 2D area scan, were analysed using the HyperSpy (de la Peña et al., 2019) Python library. The diffraction data were decomposed using an unsupervised machine learning algorithm based on non-negative matrix factorization, and subsequently matched with phases of the Al–Mg–Si–Cu system (Sunde *et al.*, 2018).

Results and discussion

Figure 1 shows the evolution of the alloy microstructure after exposure to subsequent stages of heating. The time–temperature evolution is indicated in schematic B, showing the times (t_x) at which bright-field images and SPED scans were obtained. In the initial stages ($t_1 - t_3$), the needle-shaped character of the majority of precipitates was hard to discern, and many likely existed as small atomic clusters or Guinier–Preston zones. Dislocations and surface impurities introduced by FIB (dark regions of Figs. 1C,D) gradually annealed out. At t_4 (image E), the needle morphology was clearly visible, and a high density of small precipitates had formed. The thermal exposure at this point corresponded with near peak hardness in isothermally heated bulk specimens. Figure 2 shows the phase mapping results obtained from SPED data. Figure 2(A) was constructed from SPED scan1 acquired at t_4, and shows that the majority of precipitates in the region were β''. There was also a significant presence of *L*-phase and β'/*Q*′-phase precipitates.

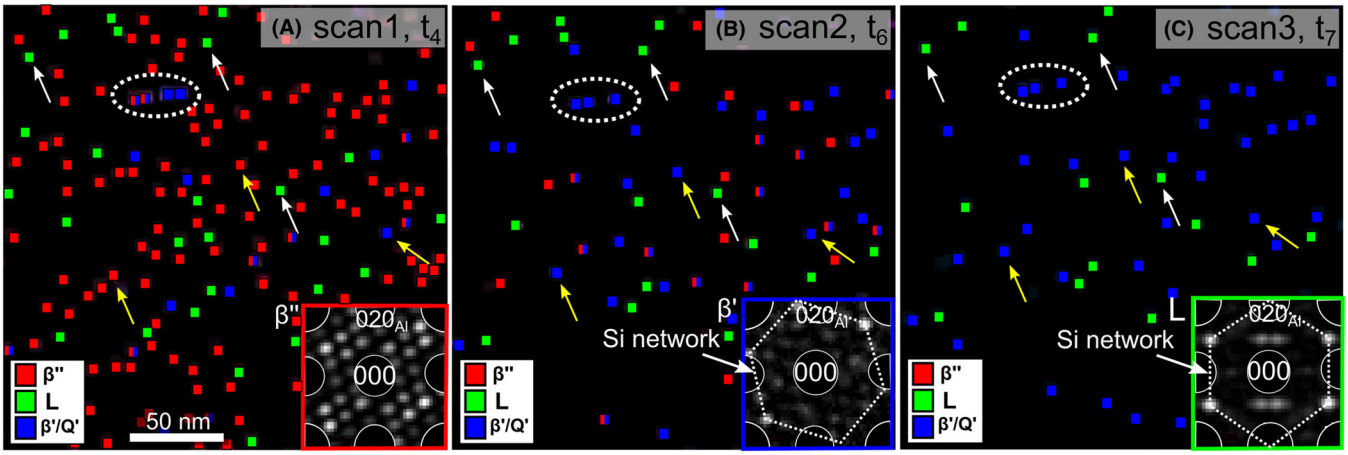

Fig. 2. (A–C) Phase maps constructed from SPED scan decomposition results. The inserts show decomposition component patterns matched with indicated phases.

Table 1. Precipitate statistics and proportion of the total volume fraction of precipitate phases existing in the microstructure after isothermal ageing at 180°C conducted *ex situ* and *in situ*.

Condition	Needle length (nm)	Number density (#/μm^3)	β'' (%)	L (%)	β'/Q' (%)	U2 (%)
3 h *ex situ*	11.2 ± 0.6	$(10.7 \pm 1.1) \times 10^4$	69 ± 5	12 ± 2	11 ± 2	8 ± 3
4.3 h *in situ* (t_4)	8.4 ± 0.8	$(13.5 \pm 1.5) \times 10^4$	72 ± 5	13 ± 3	15 ± 3	–
24 h *ex situ*	13.0 ± 1.0	$(8.0 \pm 0.8) \times 10^4$	47 ± 4	21 ± 2	24 ± 2	8 ± 3

After subsequent heating stages at $T > 180$°C the precipitates coarsened and subsequently dissolved. The phase map in Figure 2(B) at t_6 shows a low presence of remaining β'' precipitates, and at time t_7 (Fig. 2C), there were none left. At this stage, there were only *L*-phase and β'/Q'-phase precipitates present. The six precipitates indicated by white and yellow arrows that existed throughout the full heating experiment support current hypotheses regarding the precipitation in this alloy system: The *L*-phase precipitates remained fixed as *L* phases through the full experiment, and could be traced back to 1 h ageing (not shown). This observation indicates that this phase exhibits a separate evolution, likely tracing back to the clustering stage. No new *L*-phase precipitates were formed. The high thermal stability of this phase was also clearly demonstrated, as the majority of the *L*-phase precipitates at t_4 remained at t_6 and t_7 (Marioara *et al.*, 2014). Two out of three yellow marked precipitates started out as β'' precipitates (t_4), but were at t_6 seen to have transformed to β', in agreement with established knowledge about the precipitation in these alloys (Edwards *et al.*, 1998; Marioara *et al.*, 2007). The surrounding β'' precipitates at t_4 which were subsequently dissolved are thought to free solute to the matrix surrounding the evolving β' precipitates.

Table 1 shows a comparison of measured precipitate statistics at time t_4 to that of *ex situ* heated specimens studied after 3 and 24 h isothermal ageing at 180°C, corresponding with a peak-hardened and a slightly overaged condition, respectively. Bright-field images of the material microstructures for the conditions listed in Table 1 are shown in Figure 3. It is observed that the precipitate statistics in the studied region of the *in situ* heated lamella (thickness ~ 90 nm) showed a more refined microstructure of smaller precipitates relative to the isothermally heated bulk specimens. This indicated that the material was still in an underaged state. This is thought to have occurred primarily due to a lack of solutes which instead have diffused towards the top and bottom surfaces of the TEM lamella. It has previously been shown that there was a significant migration of Si and Mg to the surface of an Al–Mg–Si–Li alloy at 200°C, with concentrations exceeding 10 at.% for both atomic species in the top nanometre of the specimen (Cooil *et al.*, 2016). Mg was shown to migrate towards grain boundaries (GBs), whereas Si was ubiquitous. It is important to note that the surface oxide was removed by Ar^+ bombardment in the cited study. The specimen in the present study was exposed to air before insertion into the TEM, and therefore formed several nanometre thick surface oxide layers. Due to the similarities in element additions and temperature, surface segregation of solutes is also thought to have occurred for the alloy studied in this work. Decreased levels of precipitate forming elements, most notably Si, are thought to be the main reason for the observed reduction in precipitate growth as compared to specimens prepared

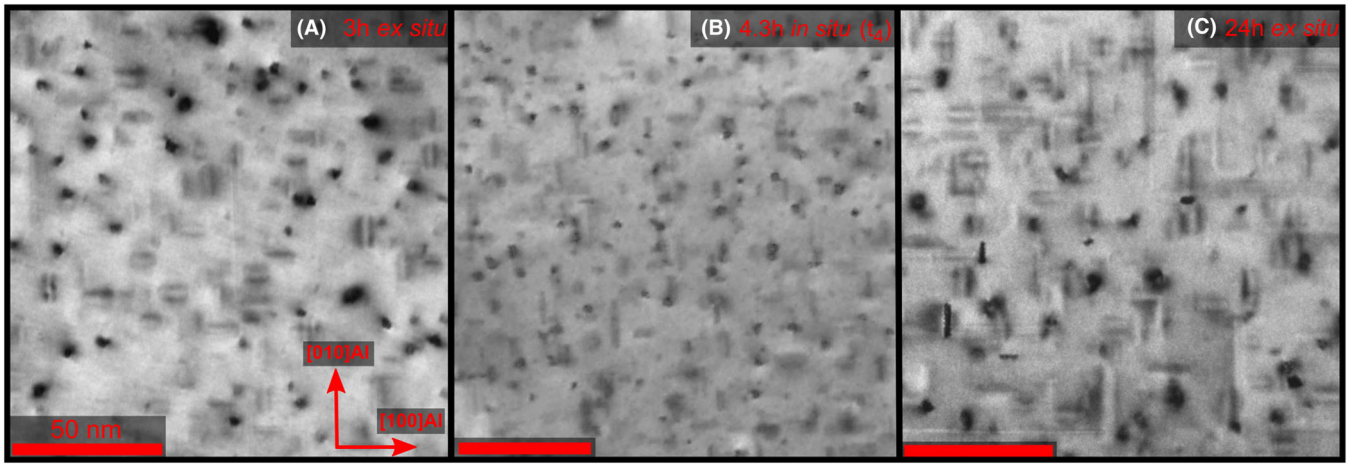

Fig. 3. (A–C) Bright-field TEM images of the alloy microstructures after (A) 3 h *ex situ*, (B) 4.3 h *in situ* and (C) 24 h *ex situ* ageing at 180°C. All scale bars equal 50 nm.

from bulk conditions. In addition, because the TEM lamella is free to bend and expand in one dimension, different from a bulk material, strain relaxation could also have contributed to reduced precipitate growth. Heterogeneous nucleation of precipitates in cold worked materials is known to accelerate precipitation significantly, with dislocations acting as high-diffusion pathways. However, as the bulk material was not subjected to any cold deformation and the resulting division of precipitate types formed was similar, the effect is thought to be less important than surface segregation of solutes.

The precipitates in the studied region did not grow larger than 30 nm in length (see Fig. 1H). In a thicker region of the specimen (Fig. 1J, ~130 nm thickness), some precipitates grew to reach above 100 nm in length, similar to significantly overaged conditions in the isothermally aged bulk material (Sunde *et al.*, 2019). There is a striking difference between the scarcely populated region of Figure 1(I) to that of Figure 1(J), both acquired at the same condition. The dissolution of precipitate phases in a thin region of the lamella further indicated that the concentration of solutes (and potentially vacancies) in the specimen had developed in a significantly different manner than for the bulk material.

As the material was pre-aged before FIB specimen preparation, the vacancy concentration was likely near equilibrium concentration initially. Before *in situ* ageing, below the surface oxide layers, the top and bottom surfaces of the material were rich in dislocations and Ga^+ ions from the FIB. Metal/amorphous interfaces serve as dislocation sinks (Legros *et al.*, 2009; De Knoop & Legros, 2014), and the initial bright-field imaging observations showed that the dislocations and surface impurities were annealed out after a relatively short time. It is not known whether the metal/oxide interfaces act as net sources or sinks of vacancies. *In situ* observations of precipitate-free zones (PFZs) surrounding dispersoids near the studied region showed that the PFZs grew at similar rates as for PFZs surrounding dispersoids and GBs in the bulk material. The comparable growth rates are taken as a qualitative indication that the concentration of vacancies in the lamella was comparable to that of the bulk material.

Our hypothesis regarding precipitate dissolution is that with a driving force causing solutes to segregate to the specimen surfaces with ageing, the precipitates that were positioned near or grew to reach in proximity of the surfaces dissolved, thus initiating the formation of PFZs. Subsequently, the continued segregation of solutes to the surfaces lead to further growth of the PFZ regions, and the growing PFZs reached precipitate phases buried progressively deeper in the lamella thickness, causing further dissolution. In addition, the lack of solutes through the lamella thickness might eventually have caused dissolution of the remainder precipitate phases. High-resolution high-angle annular dark-field scanning TEM imaging was attempted at t_5, but the precipitates were buried too deep in the material to be imaged, which supports the PFZ hypothesis. Future experiments will attempt SHT and re-ageing *in situ* to see whether the experiment can be repeated on the same lamella. Thickness effects will also be studied more carefully to assess the transferability of the results to bulk precipitation behaviour.

Conclusions

The high thermal resistance of the *L* phase was demonstrated, being one of the main phases remaining after multiple stages of high thermal exposure (180–240°C). β'' was the main precipitate phase near peak-hardened conditions, and formed a high number density of precipitates. A few percentage of the β'' precipitates subsequently transformed to β'/Q' phases, whereas the rest dissolved. Specimen thickness had a pronounced effect on the ageing kinetics, and additional experiments comparing *in situ* and *ex situ* heating TEM results are necessary to investigate this aspect further.

Acknowledgements

The authors acknowledge support from the AMPERE project (NFR 247783), a knowledge building project for industry, cofinanced by the Research Council of Norway (NFR), and the industrial partners Hydro, Gränges, Neuman Aluminium Raufoss (Raufoss Technology) and Nexans. The (S)TEM work was carried out on the NORTEM infrastructure (NFR 197405) at the TEM Gemini Centre, Trondheim, Norway.

Conflict of interest

The authors declare no conflict of interest.

References

Chang, C.S.T., De Geuser, F. & Banhart, J. (2015) In situ characterization of β'' precipitation in an Al-Mg-Si alloy by anisotropic small-angle neutron scattering on a single crystal. *J. Appl. Crystallogr.* **48**, 455–463. https://doi.org/10.1107/S1600576715002770.

Cooil, S.P., Mørtsell, E.A., Mazzola, F. *et al.* (2016) Thermal migration of alloying agents in aluminium. *Mater. Res. Exp.* **3**(11). https://doi.org/10.1088/2053-1591/3/11/116501.

De Knoop, L. & Legros, M. (2014) Absorption of crystal/amorphous interfacial dislocations during in situ TEM nanoindentation of an Al thin film on Si. *Scr. Mater.* **74**, 44–47. https://doi.org/10.1016/j.scriptamat.2013.10.003.

de la Peña, F., Prestat, E. Fauske, V.T. et al. (2019) Hyperspy/hyperspy: v1.5.2. https://doi.org/10.5281/zenodo.3396791.

Edwards, G.A., Stiller, K., Dunlop, G.L. & Couper, M.J. (1998) The precipitation sequence in Al-Mg-Si alloys. *Acta Mater.* **46**(11), 3893–3904. https://doi.org/10.1016/S1359-6454(98)00059-7.

Flament, C., Ribis, J., Garnier, J. *et al.* (2017) Stability of β'' nano-phases in Al-Mg-Si(-Cu) alloy under high dose ion irradiation. *Acta Mater.* **128**, 64–76. https://doi.org/10.1016/j.actamat.2017.01.044.

Legros, M., Cabié, M. & Gianola, D.S. (2009) In situ deformation of thin films on substrates. *Microsc. Res. Technol.* **72**(3), 270–283. https://doi.org/10.1002/jemt.20680.

Liu, C., Malladi, S.K., Xu, Q., Chen, J., Tichelaar, F.D., Zhuge, X. & Zandbergen, H.W. (2017) In-situ STEM imaging of growth and phase change of individual $CuAl_X$ precipitates in Al alloy. *Sci. Rep.* **7**, 2184. https://doi.org/10.1038/s41598-017-02081-9.

Malladi, S.K., Xu, Q., Van Huis, M.A. *et al.* (2014) Real-time atomic scale imaging of nanostructural evolution in aluminum alloys. *Nano Lett.* **14**(1), 384–389. https://doi.org/10.1021/nl404565j.

Marioara, C.D., Andersen, S.J., Røyset, J., *et al.* (2014) Improving thermal stability in Cu-containing Al-Mg-Si Alloys by precipitate optimization. *Metal. Mater. Trans. A* **45**(7), 2938–2949. https://doi.org/10.1007/s11661-014-2250-0.

Marioara, C.D., Andersen, S.J., Stene, T.N., Hasting, H., Walmsley, J., van Helvoort, A.T.J. & Holmestad, R. (2007) The effect of Cu on precipitation in Al-Mg-Si alloys. *Philos. Mag.* **87**(1), 3385–3413. https://doi.org/10.1080/14786430701287377.

Park, J., Kamachali, R.D., Kim, S.D., Kim, S.H., Oh, C.S., Schwarze, C. & Steinbach, I. (2019) First evidence for mechanism of inverse ripening from in-situ TEM and phase-field study of δ' precipitation in an Al-Li alloy. *Sci. Rep.* **9**(1), 1–11. https://doi.org/10.1038/s41598-019-40685-5.

Sunde, J.K., Marioara, C.D. & Holmestad, R. (2019) The effect of low Cu additions on precipitate crystal structures in overaged Al-Mg-Si(-Cu) alloys. *Submitted.*

Sunde, J.K., Marioara, C.D., van Helvoort, A.T. & Holmestad, R. (2018) The evolution of precipitate crystal structures in an Al-Mg-Si(-Cu) alloy studied by a combined HAADF-STEM and SPED approach. *Mater. Charact.* **142**(1), 458–469. https://doi.org/10.1016/j.matchar.2018.05.031.

Tsao, C.S., Chen, C.Y., Jeng, U.S. & Kuo, T.Y. (2006) Precipitation kinetics and transformation of metastable phases in Al-Mg-Si alloys. *Acta Mater.* **54**(17), 4621–4631. https://doi.org/10.1016/j.actamat.2006.06.005.

